Thin SnO_2 Nanowires with Uniform Diameter as Excellent Field Emitters: A Stability of More Than 2400 Minutes

Xiaosheng Fang, Jian Yan, Linfeng Hu,* Hui Liu, and Pooi See Lee*

The stability of a field-emission event, i.e., the stability of the emission current over a long period of time, against thermal effects, etc., is one of the key factors for its application in real devices. Although nanostructures have the advantages of high aspect ratios and faster device turn-on times, the small masses and large surface areas make them vulnerable to both chemical and physical damages and they have a lower melting point compared to bulk materials of same compositions. SnO_2, one of the most attractive oxide semiconductors, which has with a relatively low work function of 4.7 eV, has been a perspective candidate for field emitters. A highly stable field emitter based on thin and quasi-aligned SnO_2 nanowire ensembles with uniform diameter is shown. Field-emission measurements of these SnO_2 nanowire ensembles show low turn-on and threshold voltages of 3.5 V μm^{-1} and 4.63 V μm^{-1}, respectively, at an anode–sample distance of 200 μm and very long term scale stability of more than 2400 min, acquired at the electric field of 4.65 V μm^{-1}. Such values are not only better than those of the recently developed SnO_2 nanostructures with different morphologies and of randomly oriented SnO_2 nanowire ensembles with a similar diameter distribution, but also comparable with the most widely studied field-emission materials, such as carbon nanotubes and ZnO nanostructures. The potential for using these thin SnO_2 nanowire ensembles with uniform diameter in field emitters is shown, with particular promise in those operated for long-term real device applications.

1. Introduction

One-dimensional (1D) inorganic semiconductor nanostructures, such as nanowires, nanobelts, and nanotubes, are not only attracting tremendous interest due to their unique physical and chemical properties intrinsically associated with their low dimensionality and the quantum confinement effect,[1–5] but also offer several unique features for numerous applications because of their precisely controlled size, shape, interfacial properties, and photochemical and electronic properties.[6–10] Due to their high surface-to-volume ratios and rationally designed surfaces, 1D inorganic semiconductor nanostructures can be used as the ideal building blocks for constructing high-performance nanodevices, such as field emitters,[11] solar cells,[12] lasers diodes,[13] field-effect transistors,[14] optoelectronic sensors, and piezo nanogenerators.[15–17]

Field emission (FE, also known as electron field emission) is an emission of electron that is induced by external electromagnetic fields. In the case of a nanostructure, it has the advantage of faster device turn-on time, compactness, and sustainability compared to conventional bulky technologies.[18] It is generally accepted that the intrinsic field enhancement of an individual nanowire is approximately proportional to its aspect ratio (length-to-radius ratio).[19] It has been demonstrated that field-emission performance of a given material can be effectively optimized by increasing its aspect ratio. For example, Ren and co-workers observed enhanced field-emission from ultralong ZnO nanobelts with increasing aspect ratio.[19] Ultrafine ZnS nanobelts with high aspect ratios have been demonstrated to be excellent field emitters with a relatively low turn-on field and a high field-enhancement factor, although the work function of ZnS (7.0 eV) is larger than many other inorganic semiconductors.[20]

Tin dioxide (SnO_2) is an n-type, wide-bandgap, metal-oxide semiconductor with a direct bandgap of ≈3.6 eV.[21] 1D SnO_2 nanostructures with various morphologies have been commonly used as the detecting element in effective gas sensors and are ideal building blocks for nanoscale optoelectronic devices.[22–25] With a relatively low work function of 4.7 eV, compared with other field-emission materials such as C nanotubes (5.0 eV), ZnO (5.3 eV), ZnS (7.0 eV), SnO_2 is also a potential candidate for field emitters. However, until now, the studies on the FE properties of SnO_2 nanostructures have been rather limited compared to other field emitters such as carbon nanotubes and ZnO nanomaterials.[19] Although the field emission properties of 1D SnO_2 nanobelt arrays as well as rod-shaped and wire-shaped SnO_2 nanowhiskers have been reported,[26–29] the performance of these field-emitters should be further improved; in particular the FE stability, i.e., stability of the emission current over a long period of time, should be enhanced.

Prof. X. S. Fang, Dr. L. F. Hu, H. Liu
Department of Materials Science, Fudan University
Shanghai 200433, P. R. China
E-mail: xshfang@fudan.edu.cn; hlf11@fudan.edu.cn
Dr. J. Yan, Prof. P. S. Lee
Temasek Laboratories
Nanyang Technological University (NTU), 637553, Singapore
Prof. P. S. Lee
School of Materials Science and Engineering
NTU, 50 Nanyang Avenue, 639798, Singapore

DOI: 10.1002/adfm.201102196

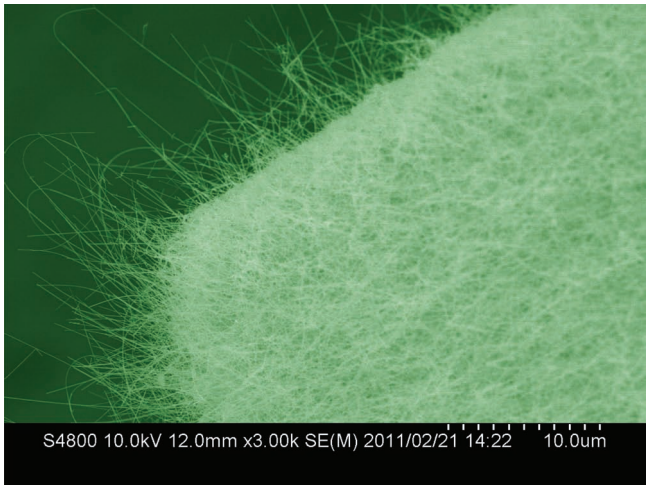

Figure 1. SEM image of the as-synthesized SnO_2 product, displaying quasi-aligned wire-like nanostructures.

Very recently, we have demonstrated that an ultraviolet photodetector based on thin SnO_2 nanowires with uniform diameter exhibits an ultrahigh external quantum efficiency of 1.32×10^7. The typical length of the nanowires is approximately 30–40 μm, with uniform diameter.[30] Motivated by these results and the unique advantages of ultrahigh aspect ratio of the SnO_2 nanowires, here we report their FE properties. This shows that the long and thin SnO_2 nanowires with uniform diameter are good field emitters with low turn-on and threshold voltages of 3.5 V μm^{-1} and 4.63 V μm^{-1}, respectively, and particularly good long-term stability of more than 2400 min. The excellent field-emission characteristics suggest the use of such nanostructures as building blocks is expected to play crucial roles in future nanodevices.

2. Results and Discussion

The as-synthesized sample was first characterized by scanning electron microscopy (SEM) and X-ray diffraction (XRD) to demonstrate the high purity, high yield, and structural control. **Figure 1** shows the typical SEM image of the product. A large quantity of quasi-aligned wire-like nanostructures can be found, which is similar what is shown in Figure 1b of ref [30]. The observations reveal that a typical length of the wires is about 30 to 40 μm. XRD measurements indicated that the products are high purity tetragonal rutile structure without impurities.[30] **Figure 2**a,b shows high-magnification SEM and transmission electron microscopy (TEM) images. It is clearly shown that the wire-like morphology and the nanowires have smooth surfaces and uniform dimensions across their entire length. There is evidence that the diameters of these SnO_2 nanowires show a narrow distribution. A statistical measurement was carried out and a Gaussian distribution result is shown in Figure 2c. Such narrow diameter distribution, high aspect ratio, and surface-to-volume ratio of the nanowires are always expected for high-performance field emitters with good stability, low turn-on

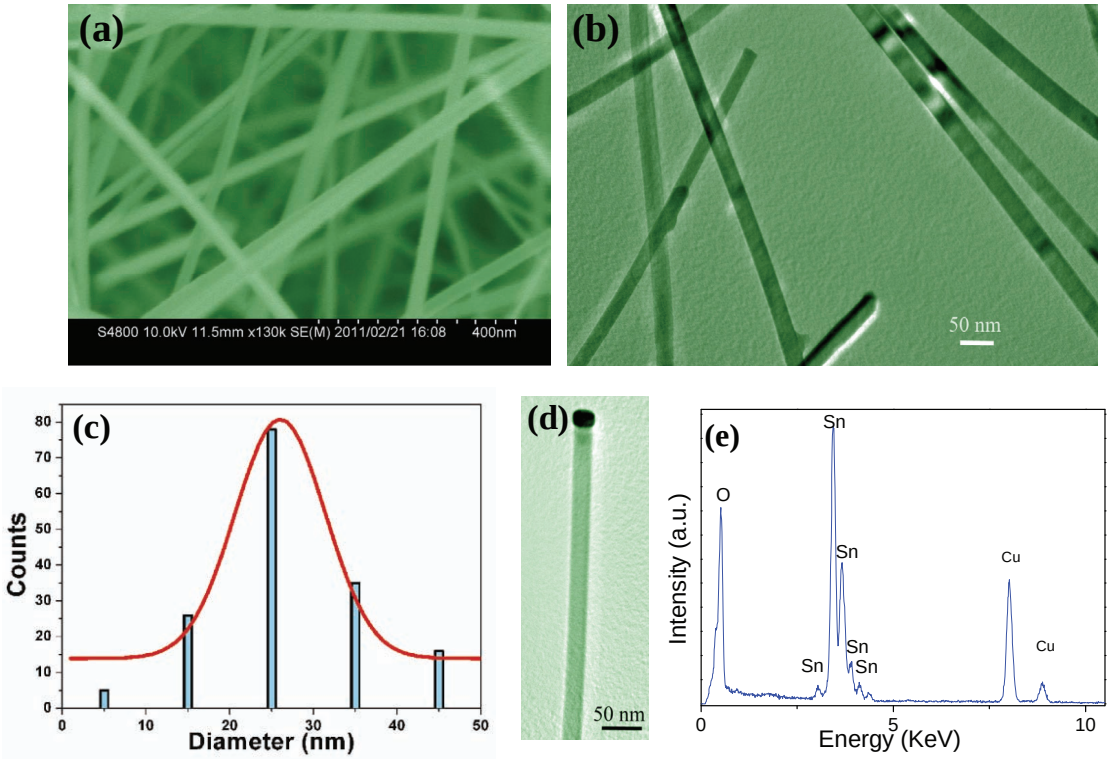

Figure 2. a,b) High-magnification SEM and TEM images of SnO_2 nanowires, respectively. c) A statistical distribution of the nanowire diameters. The red line shows the Gaussian fit. d) A typical TEM image of a single SnO_2 nanowire with a tip-end nanoparticle and e) the corresponding EDS spectrum of the nanowire stem.

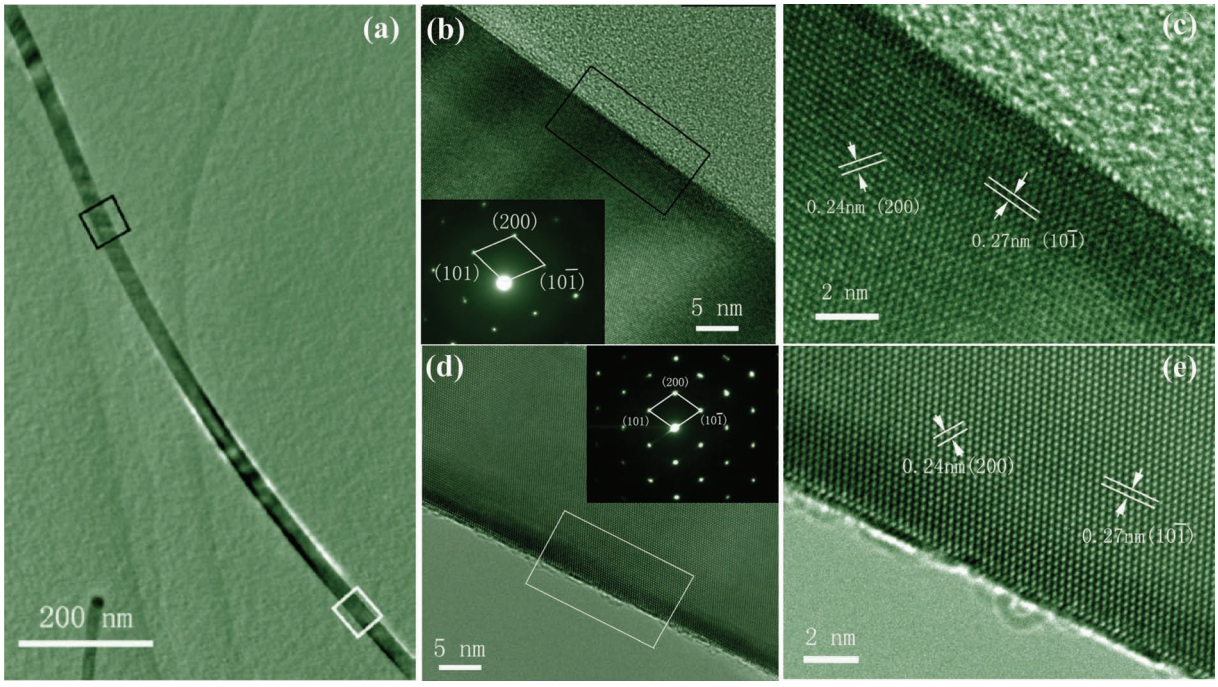

Figure 3. a) TEM image of a single SnO_2 nanowire with a typical diameter of ≈25 nm. b) High-magnification TEM image of the part labeled with black rectangle in (a). The inset shows the corresponding SAED pattern; the electron beam is parallel to [010] direction. c) An enlarged lattice-resolved HRTEM image taken from the black rectangle-labeled area in (b). d) High-magnification TEM image of section marked with white rectangle in (a). The inset shows the corresponding SAED pattern. e) An enlarged lattice-resolved HRTEM image taken from the white rectangular marked area in (d).

and threshold fields, and high field enhancement factors (β).[18] Figure 2d shows a typical image of a single nanowire with a diameter of about 23.0 nm, in which a nanoparticle was found on the tip of the nanowire. It suggests that the growth of SnO_2 nanowires follows the vapor–liquid–solid (VLS) mechanism, as reported previously.[31] The corresponding X-ray energy-dispersive spectroscopy (EDS) spectrum acquired from the nanowire stem in Figure 2d confirms that the nanowire consists of Sn and O with a stoichiometric SnO_2 composition. The Cu peaks are caused by the TEM grid.

A representative structural characterization of individual SnO_2 nanowires is presented in **Figure 3**. Two segments, marked with rectangles (Figure 3a), were chosen to study the crystal structure. Figure 3b shows a high-resolution TEM (HRTEM) image of the part labeled with black rectangle in Figure 3a, and the inset illustrates the corresponding selected-area electron diffraction (SAED) pattern, which suggests that the SnO_2 nanowire has a tetragonal phase. The sharp contrast of the diffraction dots indicates that the nanowire is highly crystallized. This is further demonstrated by the enlarged lattice-resolved HRTEM image (Figure 3c), which reveals a clear 2D lattice fringe that is free of defects. The marked spacings of ≈0.24 and ≈0.27 nm of the lattice fringe correspond to the distances of (200) and (10$\bar{1}$) planes of the tetragonal SnO_2, respectively. The other segment, marked with white rectangles in Figure 3d,e, gives similar results. These confirm that the whole SnO_2 nanowire is single-crystalline with high-quality and uniform microstructures. It is also noted that the growth direction of the present SnO_2 nanowire is different from that of our previously reported one.[30] The <101> directions are equivalent in the crystallography of tetragonal SnO_2. As the surface energies between (101) and (10$\bar{1}$) are quite similar, a slight fluctuation of the reaction conditions might induce a change in the growth direction.[32] It is rational to identify that the SnO_2 nanowires with the two growth directions both exist in our sample, which was confirmed by detailed HRTEM observations.

A detailed chemical analysis was carried out using elemental mappings and line-scanning elemental mapping. **Figure 4** shows a typical scanning transmission electron microscopy (STEM) image of a single-crystalline SnO_2 nanowire and the corresponding elemental maps, demonstrating that Sn and O are homogeneously distributed within each individual nanowire. At the initial tip, an Au nanoparticle could clearly be observed and acts as the catalyst to guide the growth (Figure 4d). The average diameter of the nanowire is close to the size of the gold particle. Line-scanning (indicated by a line in **Figure 5**a) elemental mapping of the gold nanoparticle was performed and the result is shown in Figure 5b. Low amounts of Sn and O were detected. These results demonstrate undoubtedly that the growth of SnO_2 nanowires is dominated by the VLS mechanism. The enlarged lattice-resolved HRTEM image of the interface is shown in Figure 5c. The marked d-spacings of ≈0.24 nm and ≈0.24 nm correspond to the distances of Au (111) planes and SnO_2 (020) planes, respectively. Such low lattice mismatch allows an epitaxial relationship between the Au and SnO_2 with little strain. That might be the reason why the Au nanoparticle shows the rectangular shape while most of the Au nanoparticles exhibit sphere-like shapes as a catalyst for the

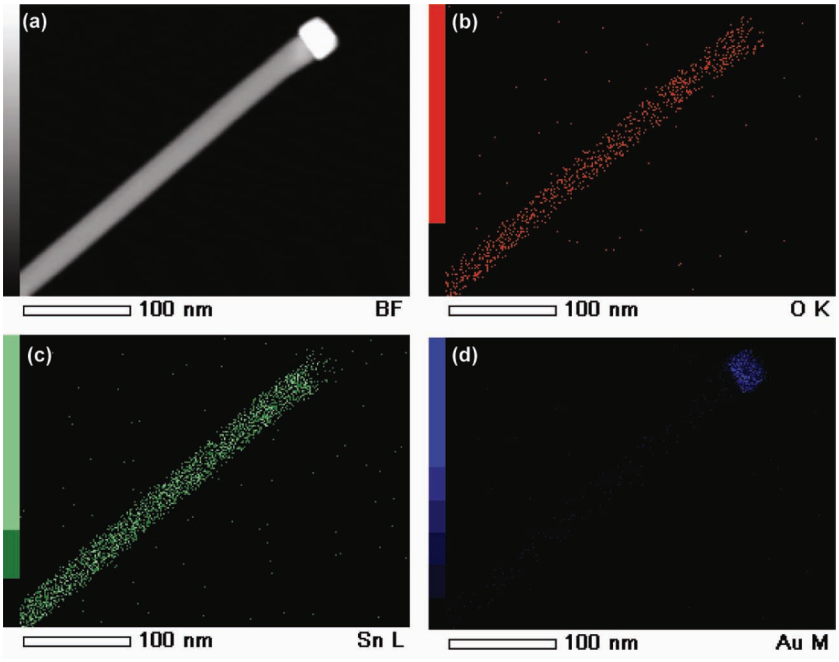

Figure 4. a) Typical high-angle annular dark field (HADDF) STEM of a single SnO_2 nanowire with a nanoparticle on the tip. b) O, c) Sn, and d) Au elemental maps for the SnO_2 nanowire in (a).

growth of nanowires.[33] It is noted that the growth direction can be identified in Figure 3c (or e) since the planes are (200) and $(10\bar{1})$. However, in Figure 5c, only the (020) plane can be clearly observed and it is difficult to identify the growth direction. Furthermore, as the (200) (Figure 3c) and (020) (Figure 5c) planes are perpendicular to each other, it is possible that the nanowires shown in the two pictures could possess the same growth direction.

As discussed above, the growth of SnO_2 nanowires is dominated by an Au-catalyzed VLS mechanism. The diameter of the SnO_2 nanowire is determined by the Au nanoparticle size. **Figure 6**a shows a typical SEM image of the Au nanoparticles obtained under the same experimental conditions with the absence of the source materials. The diameters of Au nanoparticles, which were statistically measured from 200 particles displayed, a Gaussian distribution with the maximum diameter of 12.6 ± 6.0 nm (Figure 6b). This is slightly smaller than the diameter of SnO_2 nanowires. Considering the effect of thermal expansion and formation of Au–SnO_2 alloy, the size distribution of Au nanoparticles is coincident with that of SnO_2 nanowires, which may be responsible for the narrow distribution of the SnO_2 nanowire diameters.

Twin-crystal structure with a twin boundary of the (101) plane was occasionally observed for nanowires during the TEM measurements. According to numerous HRTEM observations, the twin-crystal SnO_2 structure made up several percent of the entire product. As shown in **Figure 7**a, the SnO_2 nanowire contains two crystal domains with different contrast with a line parallel to the axial of nanowire indicating the twinning plane. The corresponding SAED pattern (Figure 7b) with the electron beam parallel to [010] direction of tetragonal SnO_2 reveals complete crystallography information. One can clearly see that two sets of electron diffraction (ED) patterns are simultaneously visible, as plotted with green and yellow colors. Further analysis indicates that the two crystal domains are structurally mirrored with respect to the central axis, which is reflected in the HRTEM image (Figure 7c). The marked interplanar *d* spacings are ≈0.24 nm and ≈0.27 nm, which correspond to the (200) and (101) lattice planes of the tetragonal SnO_2, respectively. The twin boundary can be deduced to be the (101) plane. The detailed structural relationship between the twin crystal domains is well illustrated in the structural model shown in Figure 7d, in which the combination of (200) planes can be well understood. Kinetically, the (101) and $(\bar{1}01)$ planes are identical in the growth of the crystal in the case of the tetragonal structural SnO_2 crystal.[34] In addition, the (101) and $(\bar{1}01)$ planes

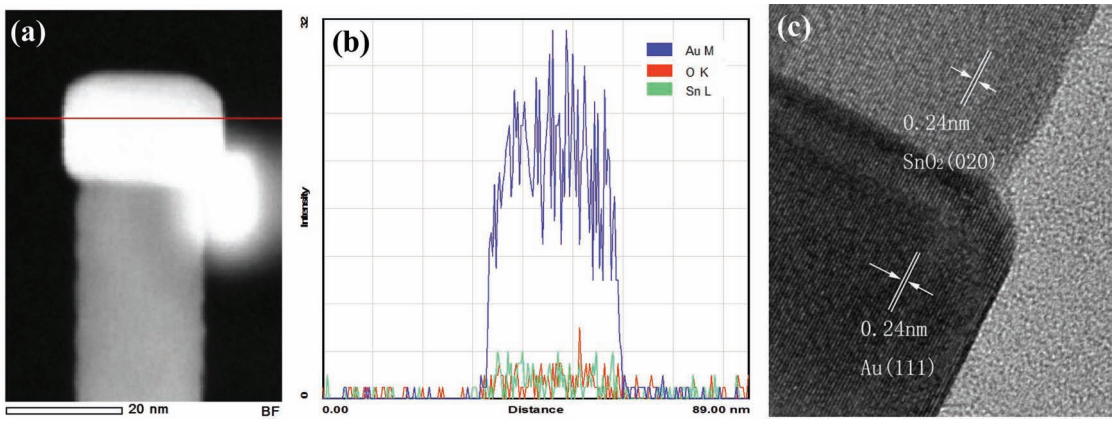

Figure 5. a) HADDF STEM image the SnO_2 with an Au nanoparticle tip. b) The corresponding EDS line scan profile across the Au nanoparticle (as indicated by the line in (a)). c) An enlarged lattice-resolved HRTEM image of the interface between the nanowire and the Au tip.

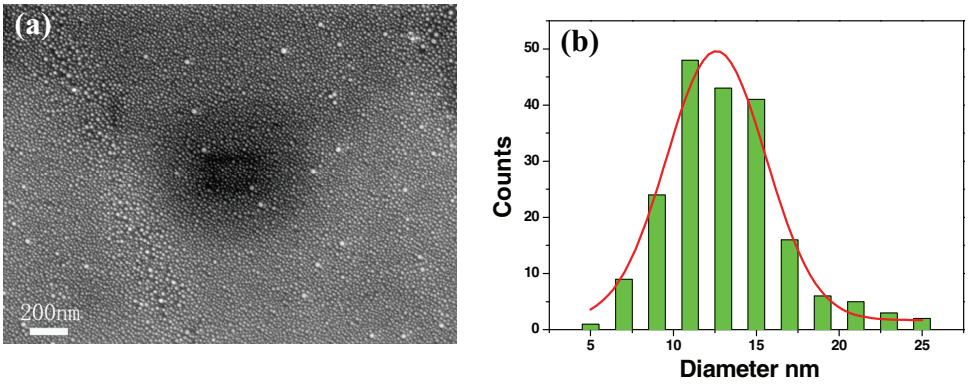

Figure 6. a) SEM image of the Au nanoparticles obtained under the same experimental conditions in the absence of source materials. b) A statistical distribution of the diameters of Au nanoparticles and the corresponding Gaussian fit.

are also close-packed and polarized planes. The [101] and [$\bar{1}$01] are both prior directions for the growth of crystal. Therefore, SnO_2 has a trend to form branched, zigzag, and spring nanostructures, as reported previously.[32,34–37] Although such a highly symmetric crystal structures have also been observed in hexagonal nanostructures, such as ZnS and GaN,[38] it is noted that to date there are few reports on the SnO_2 twinning nanowires.[39] On the basis of the structural analysis and morphology characterization above, a possible growth mechanism of the twin structure is proposed as follows. First, the SnO_2 precursors precipitate at the surface of melted Au catalysts at a high temperature to generate initial tetragonal nuclei and then the polarity of SnO_2 may lead to the preferential growth of SnO_2 nanonuclei along a given (200) plane, which shows the fastest growth rate. Under the surface tension and temperature fluctuations, the (200) planes tend to combine by accident along the (101) plane to form a symmetrical twin structure sharing the same (101) plane. With the continuous supplying of SnO_2 precursors, this structure gradually grows and is guided by a Au catalyst attached to the initial tip end.

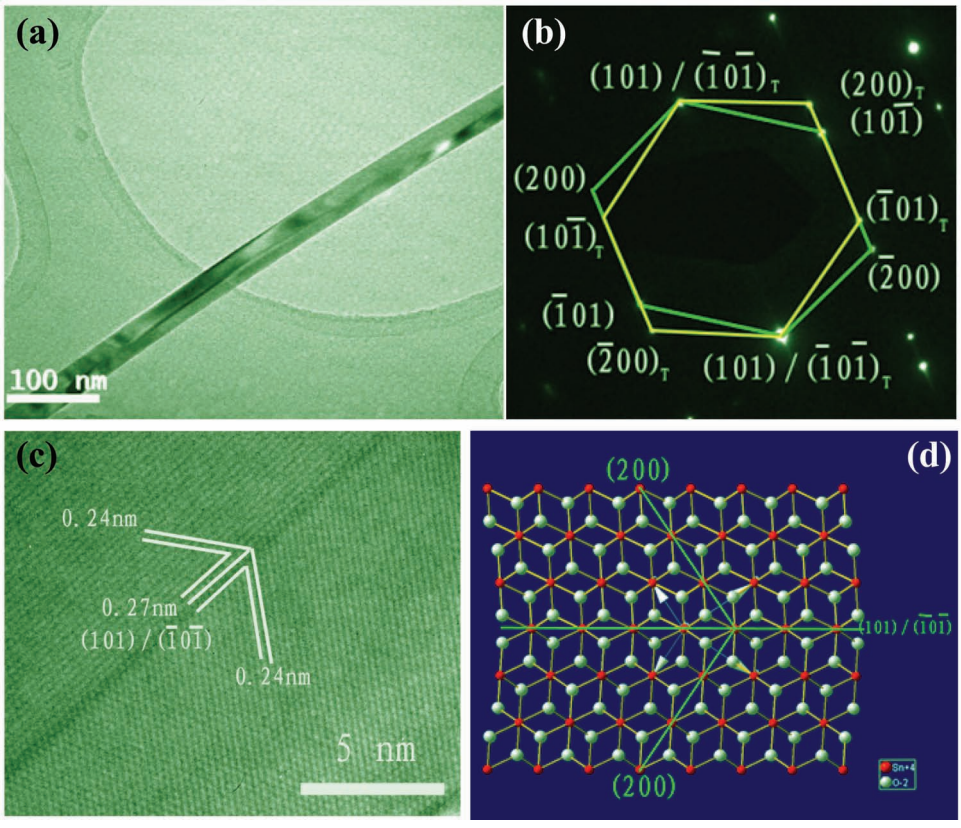

Figure 7. a) TEM image of a typical twinning SnO_2 nanowires and b) the corresponding SAED pattern. c) An enlarged lattice-resolved HRTEM image of the twinning structured nanowire. d) A schematical diagram depicting the twinning structure in the SnO_2 nanowire.

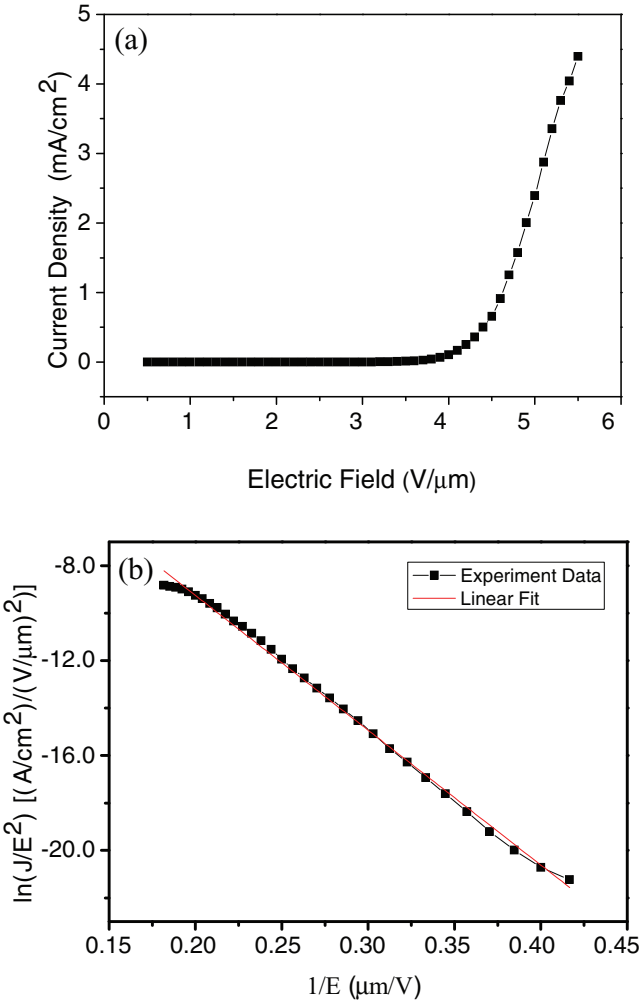

Figure 8. Field-emission properties of quasi-aligned, thin SnO_2 nanowire ensembles with uniform diameter at an anode–sample distance of 200 μm. a) A plot of the FE current density (J) versus an applied macroscopic field (E) and b) the corresponding Fowler–Nordheim $\ln(J/E^2) - (1/E)$ plot.

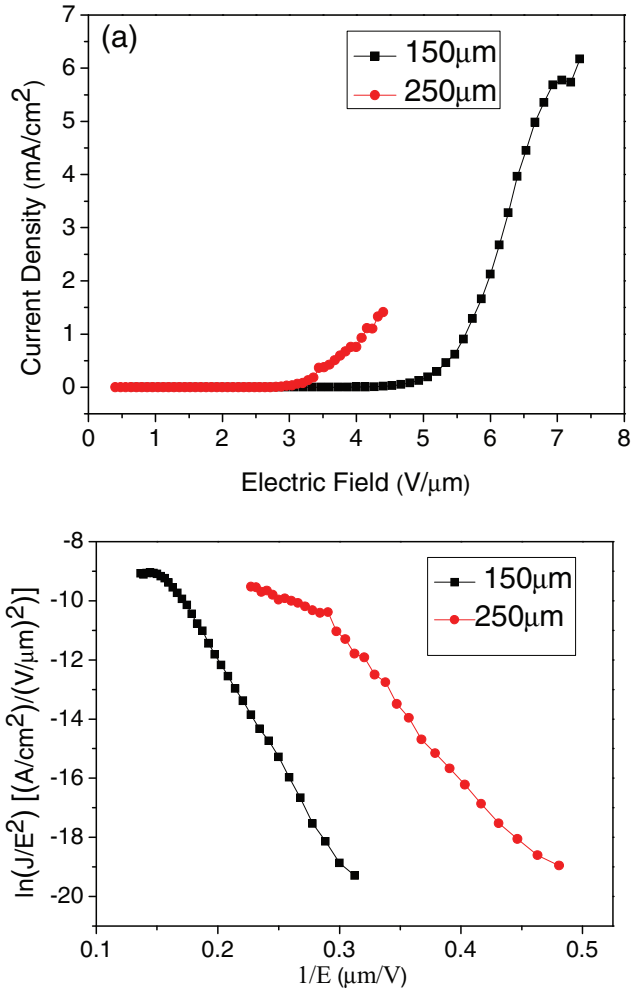

Figure 9. Field-emission properties: a) J–E curves and b) corresponding Fowler–Nordheim plots of quasi-aligned thin SnO_2 nanowire ensembles with uniform diameter at anode–cathode distances of 150 and 250 μm.

Finally, the twin-crystal SnO_2 nanowires with lengths of tens of micrometers are formed.

FE properties of the as-grown quasi-aligned SnO_2 nanowire arrays were studied in present work. **Figure 8**a depicted the emission current density versus the applied field curve (J–E) at an anode–sample distance of 200 μm from the quasi-aligned SnO_2 nanowire arrays. As can be clearly seen, the emission current density J exponentially increases with an increase of the applied field E, and the current density arrived 4.4 mA cm^{-2} when the field is 5.5 V μm^{-1}. Such a value is comparable to or even better than those of many other 1D inorganic semiconductor nanostructures or nanoarrays. For example, it was summarized that emission current densities from ZnO nanostructures rarely reached 1 mA cm^{-2} at such low electric field unless some special treatments were done, such as ion implantation and surface modifications, because these nanowires are known to barely sustain such high current and easily suffer from discharge or breakdown.[40] An emission current density of only ≈0.9 mA cm^{-2} was achieved from Si nanowire semisphere-like ensembles using a similar measurement system, even if a lower anode–sample distance of 100 μm was adopted.[41] About 1.1 mA cm^{-2} emission current density was observed from hierarchical core/shell structures consisting of primary ZnS nanotubes, In core nanowires, and ZnS nanowire secondary branches.[42] The value can be much higher at higher electric fields if the nanowires field emitters are still stable. **Figure 9** shows the field-emission properties of same zone under different anode–sample distances of 150 and 250 μm. The emission current density J reached 6.17 mA cm^{-2} at a macroscopic field of 7.33 V μm^{-1}.

Here, we define the turn-on and threshold fields as fields producing an emission current density of 10 μA cm^{-2} and 1 mA cm^{-2}, respectively. From Figure 8a, the turn-on field and threshold field for these quasi-aligned thin SnO_2 nanowire ensembles was extrapolated as 3.5 V μm^{-1} and 4.63 V μm^{-1} at an anode–sample distance of 200 μm. These values are apparently smaller than those of other SnO_2 nanostructure-based field emitters, which is very desirable for their practical applications in field emitters (as summarized in **Table 1**).[21,26–29,43,44]

Table 1. Comparison of the key FE parameters between the present thin SnO_2 nanowires with uniform diameter and the previous reports in the literature for other 1D SnO_2 nanostructures. The turn-on and threshold fields are defined as fields producing an emission current density of 10 μA cm^{-2} and 1 mA cm^{-2}, respectively. If the other values are used, it is indicated.

1D SnO_2 FEs	Turn-on field [V μm^{-1}]	Threshold field [V μm^{-1}]	Field enhancement factor (β)	Stability: testing time [h]	Reference
Nanowire	2.3 at 0.1 μA cm^{-1}	6.5	2772 at d (vacuum gap) = 200 μm	–	[28]
	3.0 at 1 mA cm^{-1}	–	–	–	[29]
	6.5 at 1 μA cm^{-1}	–	2845	–	[43]
SnO_2:Sb nanowire	4.9 at 1 μA cm^{-1}	–	3325	–	[43]
Needle-shaped nanostructures	3.3	5.5	2030 at d = 550 μm	2	[44]
Nanobelt arrays	4.5, 3.0, 2.4, and 2.3 as d is 100, 200, 350, and 500 μm at 1 μA cm^{-1}	–	950 at d = 100 μm	2	[26]
Nanograss	5.612 at 1.44 μA cm^{-1}	–	1477 at d = 446 μm	–	[27]
Zigzag nanobelts	1.9 at 0.1 μA cm^{-1}	5.1	3178 at d = 200 μm	–	[28]
Nanoroda	6.4	–	493.6 at d = 100 μm	–	[21]
Beak-like nanoroda	5.8	–	1402.9 at d = 100 μm	–	[21]
Randomly oriented nanowire ensembles with a similar diameter distrubution	3.9	>5.5	1185 at d = 200 μm	–	this work
Quasi-aligned nanowires with uniform diameters	3.5	4.63	1225 at d = 200 μm	40	this work

The quantitative description of field emitters is usually evaluated using the Fowler–Nordheim (F–N) equation: [45] $J = (A\beta^2E^2/\phi)\exp(-B\phi^{3/2}/\beta E)$or $\ln(J/E^2) = \ln(A\beta^2/\phi) - B\phi^{3/2}/\beta E$, where A and B are constants with values of 1.54×10^{-6} A eV V^{-2} and 6.83×10^3 eV$^{-3/2}$ V μm^{-1}, respectively. J is the current density, β is the field enhancement factor, E is the applied field, and ϕ is the work function of the emitting materials. Figure 8b and 9b show the F–N plots, $\ln(J/E^2)$ versus $1/E$, at different anode–sample distances (150, 200, and 250 μm). These plots show an approximately linear relationship within the measurement range, confirming the F–N behavior of the SnO_2 nanowire-based device. The field enhancement factor, β, is estimated to be 1225 in the present study (as calculated from a slope of the fitted straight line in Figure 8b). This value is comparable to the value in a previous study and more than sufficient for diverse FE applications.[19b]

Stability of the field-emitters is another important parameter for practical applications. Compared with bulk materials of the same composition, the field-emission properties are enhanced in the high-aspect-ratio 1D nanostructures. However, the small mass and large surface area of 1D nanostructures make them vulnerable to both chemical and physical damages and they have a lower melting point. As summarized in Table 1, the longest stability testing time was 2 h and most of them were blank. It was observed that the emission current density is strongly dependent on a number of factors, including the applied potential, tip geometry, the cathode material work function, etc., and therefore variations in any of these factors should be reflected in the emission currents.[19b] Long-time stability of nanostructure-based field emitters is still a challenge. Herein, FE stability measurements of the SnO_2 nanowires were performed by maintaining an electric field of 4.65 V μm^{-1} over a period of 2400 min (**Figure 10**), and no current degradations or notable fluctuations were observed during this process. Such a testing time is not only much higher than that of other SnO_2 nanostructure-based field emitters reported in the literature (Table 1), but also longer than other inorganic semiconductor nanostructures and carbon nanotubes.

The excellent FE characteristics of the SnO_2 nanowires should be attributed to their high crystallinity, high aspect

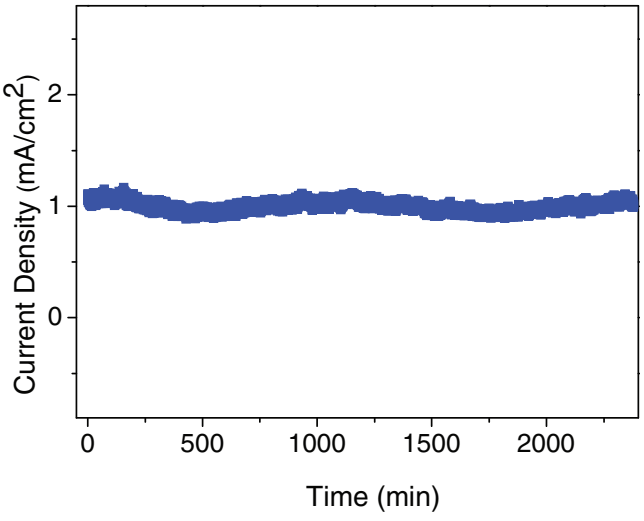

Figure 10. Field-emission current of the thin SnO_2 nanowires with uniform diameters, recorded over 2400 min with an electric field of 4.65 V μm^{-1}.

ratio, uniform 1D geometry and diameter distrubution, and quasi-aligned growth. Previous studies demonstrated that among different anisotropic structures, the one with the high aspect ratio generally exhibits superior FE performance. Compared with other 1D SnO_2 nanostructures, the thin SnO_2 nanowires exhibit an extremely high aspect ratio of more than 1000 (length of up to 30–40 μm and an average radius size only of 26 nm). The high aspect ratio or small emitter radius of the thin SnO_2 nanowires is apparently favorable for improving the performance of field emission. The narrow diameter distribution not only ensures the high aspect ratio of each SnO_2 nanowire field emitter, but also promises a long-term field-emission stability of the SnO_2 nanowire ensembles measured at a given applied electric field. It is also well known that the FE properties of a given material can be significantly optimized by fabricating aligned nanostructures with a high packing density.[19,46] The quasi-aligned distrbution of the present thin SnO_2 nanowire ensembles is also one of the favorable factors. **Figure 11** shows the field-emission properties of a randomly oriented SnO_2 nanowire ensemble with a similar diameter distribution at a 200 μm anode–cathode distance. These randomly oriented SnO_2 nanowires were formed within a relatively small zone (≈4 mm × 2 mm) at the end of the downstream direction along the same substrate (≈2 cm × 1 cm) in Figure 1. A typical SEM image shown in Figure 11a reveals that the morphology and diameter distribution are almost same, while the quasi-aligned distribution changed into a randomly oriented one. Field-emission measurements (Figure 11) reveal that the randomly oriented SnO_2 nanowire ensemble possesses a turn-on field equal to 3.9 V μm^{-1} and a threshold field of >5.5 V μm^{-1}. The emission current density is about 0.67 mA cm^{-2} when the applied macroscopic field is 5.55 V μm^{-1}. The field emhancement factor β was found to be 1185 at a working anode–sample distance of 200 μm. It is clear from all the above paramters obtained under the same measurement conditions that the quasi-aligned distrbution is beneficial for the excellent field-emission properties achieved. Previous reports suggested that the interface between the amorphous surface layer and the crystalline core may result in a strong electron scattering and thus deteriorate the FE properties of the as-grown nanostructures.[40b,47] The superior quality of the SnO_2 nanowires with a single crystal structure is also one of the key factors for the present excellent field-emission properties. Previous studies demonstrated that higher conductivity of the materials resulted in better field emission performance.[40a] The low turn-on field and threshold field, high field enhancement factor, and excellent emission stability indicate that the present SnO_2 nanowires are promising candidates for applications in cold-cathode-based electronic devices. Additionally, our previous reseach on branched ZnS nanotube/In nanowire core/shell heterostructures demonstrated that multiply enhanced field-emission properties were achieved on the basis of a sequential stepwise enhancement mechanism involving the consecutive stem and branch contributions,[42] so it is possible to optimize further the field-emission properties by constructing a hierarchical/branch structure based on the present thin SnO_2 nanowires with uniform diameter.

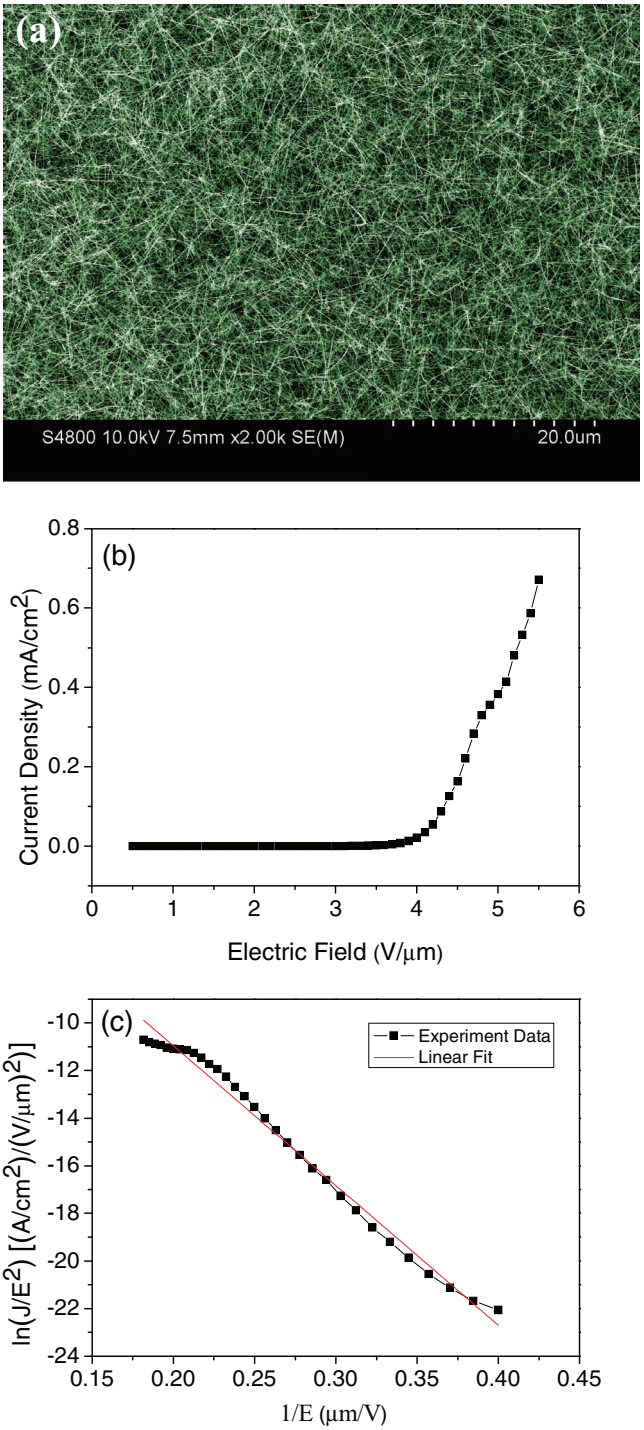

Figure 11. Morphology and field-emission properties of the as grown SnO_2 nanowires at the end of the downstream zone along the same substrate in Figure 1: a) typical SEM image, revealing a randomly oriented nanowire ensemble with a similar diameter distribution, b) *J–E* curves, and c) corresponding F–N plots at a 200 μm anode–cathode distance.

3. Conclusion

In conclusion, quasi-aligned and highly crystallized SnO_2 nanowire arrays with uniform diameter were successfully synthesized by a facile VLS process. The as-prepared SnO_2 nanowires

have lengths of up to 30–40 μm and uniform diameters of about 26 nm, exhibiting an extremely high aspect ratio and surface-to-volume ratio. Twin-crystal structure with a twin boundary of the (101) plane was occasionally observed for some nanowires. FE measurements of the thin SnO_2 nanowire ensembles with uniform diameter showed low turn-on and threshold voltages of 3.5 V μm^{-1} and 4.63 V μm^{-1}, respectively, at an anode–sample distance of 200 μm and, notably, a long-term stability more than 2400 min. Such good device performance for the thin SnO_2 nanowires with uniform diameter not only suggests that such nanowire ensembles have potential in next-generation field emitters, but also the study offers a universal and low-cost method to build field emitters with long-term stability.

4. Experimental Section

The synthesis of SnO_2 nanowires was carried out in a horizontal quartz tube furnace system using a method similar to that previously reported.[30] Mixed SnO_2 powder and carbon powders (molar ratio 1:1) were loaded into a small quartz tube with one end open at the center of the furnace. Before heating, the system was pumped to 1.4×10^{-2} mbar. Then the central temperature was increased to 910 °C at a rate of 15 °C min^{-1} and kept for 30 min under a constant Ar flow of 30 standard cubic center meter (SCCM). Si substrate coated with a 3 nm thick Au film was placed in the small quartz tube in a lower temperature region (≈600 °C) to collect the products. The pressure inside the tube was 0.4 mbar during the growth process. Subsequently, the furnace was cooled to room temperature.

The morphology, phase, microstructure, and composition of the samples were determined using a field-emission scanning electron microscope (FESEM, Hitachi S-4800), a Rigaku D/max-rB X-ray diffractometer using Cu Kα radiation (XRD, $\lambda = 0.15406$ nm) in a 2θ range from 10° to 60°, and a transmission electron microscope (TEM, JEOL 2010) equipped with an X-ray energy dispersive spectrometry (EDS). The field-emission properties of the thin SnO_2 nanowire ensembles were studied at room temperature in a high vacuum chamber (2.6×10^{-6} Pa) using a 1 mm^2 cross-sectional area copper anode. A dc voltage sweeping from 100 to 1100 V was applied to the samples. The FE stability measurements were performed at an applied electric field of 4.65 V μm^{-1} over a period of 2400 min.

Acknowledgements

This work was supported by the National Natural Science Foundation of China (Grant Nos. 91123006, 51002032, and 21001028), the National Basic Research Program of China (Grant No. 2012CB932303), Shanghai Chenguang Foundation (11CG06), Shanghai Pujiang Program (11PJ1400300), Science and Technology Commission of Shanghai Municipality (11520706200), and the Programs for Professor of Special Appointment (Eastern Scholar) at Shanghai Institutions of Higher Learning and for New Century Excellent Talents in University (NCET).

Received: September 15, 2011
Published online: February 16, 2012

[1] Y. N. Xia, P. D. Yang, Y. G. Sun, Y. Y. Wu, B. Mayers, B. Gates, Y. Yin, F. Kim, H. Yan, *Adv. Mater.* **2003**, *15*, 353.
[2] H. J. Fan, W. Lee, R. Hauschild, M. Alexe, G. Le Rhun, R. Scholz, A. Dadgar, K. Nielsch, H. Kalt, A. Krost, M. Zacharias, U. Gosele, *Small* **2006**, *2*, 561.
[3] U. K. Gautam, M. Imura, C. S. Rout, Y. Bando, X. S. Fang, B. Dierre, L. Sakharov, A. Govindaraj, T. Sekiguchi, D. Golberg, C. N. R. Rao, *Proc. Natl. Acad. Sci. USA* **2010**, *107*, 13588.
[4] a) L. Li, Y. W. Yang, G. H. Li, L. D. Zhang, *Small* **2006**, *2*, 548; b) L. Li, P. Wu, X. S. Fang, T. Y. Zhai, L. Dai, M. Y. Liao, Y. Koide, H. Q. Wang, Y. Bando, D. Golberg, *Adv. Mater.* **2010**, *22*, 3161; c) T. Y. Zhai, X. S. Fang, Y. Bando, Q. Liao, X. J. Xu, H. B. Zeng, Y. Ma, J. N. Yao, D. Golberg, *ACS Nano* **2009**, *3*, 949.
[5] a) L. D. Zhang, M. Fang, *Nano Today* **2010**, *5*, 128; b) S. L. Ji, C. H. Ye, *J. Mater. Sci. Technol.* **2008**, *24*, 457.
[6] C. M. Lieber, Z. L. Wang, *MRS Bull.* **2007**, *32*, 99.
[7] X. D. Chen, G. F. Zheng, J. I. Cutler, J. W. Jang, C. A. Mirkin, *Small* **2009**, *5*, 1527.
[8] P. D. Yang, R. X. Yan, M. Fardy, *Nano Lett.* **2010**, *10*, 1529.
[9] X. S. Fang, L. M. Wu, L. F. Hu, *Adv. Mater.* **2011**, *23*, 585.
[10] J.Z. Zhang, *MRS Bull.* **2011**, *36*, 48.
[11] a) Z. G. Chen, J. Zou, D. W. Wang, L. C. Yin, G. Liu, Q. F. Liu, C. H. Sun, X. D. Yao, F. Li, X. L. Yuan, T. Sekiguchi, G. Q. Lu, H. M. Cheng, *Adv. Funct. Mater.* **2009**, *19*, 484; b) N. S. Liu, G. J. Fang, W. Zeng, H. Long, X. Z. Zhao, *J. Phys. Chem. C* **2011**, *115*, 14377.
[12] Q. F. Zhang, C. S. Dandeneau, X. Y. Zhou, G. Z. Cao, *Adv. Mater.* **2009**, *21*, 4087.
[13] X. S. Fang, T. Y. Zhai, U. K. Gautam, L. Li, L. M. Wu, Y. Bando, D. Golberg, *Prog. Mater. Sci.* **2011**, *56*, 175.
[14] H. C. Wu, Y. C. Huang, I. K. Ding, C. C. Chen, Y. H. Yang, C. C. Tsai, C. D. Chen, Y. T. Chen, *Adv. Funct. Mater.* **2011**, *21*, 474.
[15] S. Soci, A. Zhang, B. Xiang, S. A. Dayeh, D. P. R. Aplin, J. Park, X. Y. Bao, Y. H. Lo, D. Wang, *Nano. Lett.* **2007**, *7*, 1003.
[16] X. S. Fang, Y. Bando, M. Y. Liao, U. K. Gautam, C. Y. Zhi, B. Dierre, B. D. Liu, T. Y. Zhai, T. Sekiguchi, Y. Koide, D. Golberg, *Adv. Mater.* **2009**, *21*, 2034.
[17] W. Z. Wu, Y. G. Wei, Z. L. Wang, *Adv. Mater.* **2010**, *22*, 4711.
[18] a) H. J. Jeong, H. D. Jeong, H. Y. Kim, J. S. Kim. S. Y. Jeong, J. T. Han, D. S. Bang, G. W. Lee, *Adv. Funct. Mater.* **2011**, *21*, 1526; b) L. Y. Yuan, Y. T. Tao, J. Chen, J. J. Dai, T. Song, M. Y. Ruan, Z. W. Ma, L. Gong, K. Liu, X. H. Zhang, X. J. Hu, J. Zhou, Z. L. Wang, *Adv. Funct. Mater.* **2011**, *21*, 2150.
[19] a) W. Z. Wang, B. Q. Zeng, J. Yang, B. Poudel, J. Y. Huang, M. J. Naughton, Z. F. Ren, *Adv. Mater.* **2006**, *18*, 3275; b) X. S. Fang, Y. Bando, U. K. Gautam, C. H. Ye, D. Golberg, *J. Mater. Chem.* **2008**, *18*, 509.
[20] X. S. Fang, Y. Bando, G. Z. Shen, C. H. Ye, U. K. Gautam, P. M. F. J. Costa, C. Y. Zhi, C. C. Tang, D. Golberg, *Adv. Mater.* **2007**, *19*, 2593.
[21] J. H. He, T. H. Wu, C. L. Hsin, K. M. Li, L. J. Chen, Y. L. Chueh, L. J. Chou, Z. L. Wang, *Small* **2006**, *2*, 116.
[22] A. Kolmakov, Y. X. Zhang, G. S. Cheng, M. Moskovits, *Adv. Mater.* **2003**, *15*, 997.
[23] M. S. Park, G. X. Wang, Y. M. Kang, D. Wexler, S. X. Dou, H. K. Liu, *Angew. Chem. Int. Ed.* **2007**, *46*, 750.
[24] Y. J. Choi, I. S. Hwang, J. Gwan, K. J. Choi, J. H. Park, J. H. Lee, *Nanotechnology* **2008**, *19*, 095508.
[25] B. Liu, C. W. Cheng, R. Chen, Z. X. Shen, H. J. Fan, H. D. Sun, *J. Phys. Chem. C* **2010**, *114*, 3407.
[26] Y. J. Chen, Q. H. Li, Y. X. Liang, T. H. Wang, Q. Zhao, D. P. Yu, *Appl. Phys. Lett.* **2004**, *85*, 5682.
[27] B. Wang, Y. H. Yang, C. X. Wang, N. S. Xu, G. W. Yang, *J. Appl. Phys.* **2005**, *98*, 24303.
[28] J. Wu, K. Yu, L. J. Li, J. W. Xu, D. J. Shang, Y. Xu, Z. Q. Zhu, *J. Phys. D: Appl. Phys.* **2008**, *41*, 185302.
[29] L. J. Li, F. J. Zong, X. D. Cui, H. L. Ma, X. H. Wu, Q. D. Zhang, Y. L. Wang, F. Yang, J. Z. Zhao, *Mater. Lett.* **2007**, *61*, 4152.
[30] L. F. Hu, J. Yan, M. Y. Liao, L. M. Wu, X. S. Fang, *Small* **2011**, *7*, 1012.
[31] a) A. M. Morales, C. M. Lieber, *Science* **1998**, *279*, 208; b) Y. Y. Wu, P. D. Yang, *J. Am. Chem. Soc.* **2001**, *123*, 3165.

[32] J. H. Duan, S. G. Yang, H. W. Liu, J. F. Gong, H. B. Huang, X. N. Zhao, R. Zhang, Y. W. Du, *J. Am. Chem. Soc.* **2005**, *127*, 6180.
[33] B C. Orchers, D. Stichtenoth, S. Muller, D. Schwen, C. Ronning, *Nanotechnology* **2006**, *17*, 1067.
[34] J. X. Wang, D. F. Liu, X. Q. Yan, H. J. Yuan, L. J. Ci, Z. P. Zhou, Y. Gao, L. Song, L. F. Liu, W. Y. Zhou, G. Wang, S. S. Xie, *Solid State Commun.* **2004**, *130*, 89.
[35] L. H. Huang, L. Pu, Y. Shi, R. Zhang, B. X. Gu, Y. W. Du, *Appl. Phys. Lett.* **2005**, *87*, 163124.
[36] R. S. Yang, Z. L. Wang, *J. Am. Chem. Soc.* **2006**, *128*, 1466.
[37] J. R. Duan, J. F. Gong, H. B. Huang, X. N. Zhao, G. X. Cheng, Z. Z. Yu, S. G. Yang, *Nanotechnology* **2007**, *18*, 055607.
[38] a) B. D. Liu, Z. Wang, C. Y. Li, M. Gao, M. Mitome, X. Jiang, D. Golberg, *Cryst. Growth Des.* **2010**, *10*, 4143; b) D. M. Bagnall, Y. F. Chen, Z. Zhu, T. Yao, S. Koyama, M. Y. Shen, T. Goto, *Appl. Phys. Lett.* **1996**, *68*, 403.
[39] Z. R. Dai, J. L. Gole, J. D. Stout, Z. L. Wang, *J. Phys. Chem. B* **2002**, *106*, 1274.
[40] a) J. C. She, Z. M. Xiao, Y. H. Yang, S. Z. Deng, J. Chen, G. W. Yang, N. S. Xu, *ACS Nano* **2008**, *2*, 2015; b) Q. Zhao, J. Y. Gao, R. Zhu, T. C. Cai, S. Wang, X. F. Song, Z. M. Liao, X. H. Chen, D. P. Yu, *Nanotechnology* **2010**, *21*, 095701; c) C. H. Ye, Y. Bando, X. S. Fang, G. Z. Shen, D. Golberg, *J. Phys. Chem. C* **2007**, *111*, 12673.
[41] X. S. Fang, Y. Bando, C. H. Ye, G. Z. Shen, U. K. Gautam, C. C. Tang, D. Golberg, *Chem. Commun.* **2007**, 4093.
[42] U. K. Gautam, X. S. Fang, Y. Bando, J. H. Zhan, D. Golberg, *ACS Nano* **2008**, *2*, 1015.
[43] J. M. Wu, *Thin Solid Film* **2008**, *517*, 1289.
[44] L. A. Ma, T. L. Guo, *Mater. Lett.* **2009**, *63*, 295.
[45] R. H. Fowler, L. Nordheim, *Proc. R. Soc. London A* **1928**,*119*, 173.
[46] X. S. Fang, Y. Bando, C. H. Ye, D. Golberg, *Chem. Commun.* **2007**, 3048.
[47] Y. Z. Jin, W. K. Hsu, Y. L. Chueh, L. J. Chou, Y. Q. Zhu, K. Brigatti, H. W. Kroto, D. R. M. Walton, *Angew. Chem. Int. Ed.* **2004**, *43*, 5670.